Ferromagnetic order induced on graphene by Ni/Co proximity effects

Mayra Peralta, Luis Colmenarez, Alejandro Lopez, Bertrand Berche, Ernesto Medina

Ferromagnetic order induced on graphene by Ni/Co proximity effects

Mayra Peralta,[1] Luis Colmenarez,[2,1] Alejandro López,[1] Bertrand Berche,[3,1] and Ernesto Medina[1,3,4]
[1]*Centro de Física, Instituto Venezolano de Investigaciones Científicas, 21827, Caracas, 1020 A, Venezuela*
[2]*Departamento de Física, Facultad de Ciencias y Tecnología, Universidad de Carabobo, 21827, Caracas, 1020 A, Venezuela*
[3]*Groupe de Physique Statistique, Institut Jean Lamour, Université de Lorraine, 54506 Vandoeuvre-les-Nancy Cedex, France*
[4]*Yachay Tech, School of Physical Sciences & Nanotechnology, 100119-Urcuquí, Ecuador*
(Received 12 August 2016; revised manuscript received 21 October 2016; published 6 December 2016)

We build a tight-binding Hamiltonian describing Co/Ni over graphene, contemplating ATOP (a Co/Ni atom on top of each carbon atom of one graphene sublattice) and HCP (one Co/Ni atom per graphene plaquette) configurations. For the ATOP configuration the orbitals involved, for the Co/Ni, are the $d_{z^2-r^2}$, which most strongly couples to one graphene sublattice and the d_{xz}, d_{yz} orbitals that couple directly to the second sublattice site. Such configuration is diagonal in pseudospin and spin space, yielding electron doping of the graphene and antiferromagnetic ordering in the primitive cell in agreement with DFT calculations. The second, HCP, configuration is symmetric in the graphene sublattices and only involves coupling to the d_{xz}, d_{yz} orbitals. The register of the lattices in this case allows for a new coupling between nearest-neighbor sites, generating nondiagonal terms in the pseudospin space and novel spin-kinetic couplings mimicking a spin-orbit coupling generated by a magnetic coupling. The resulting proximity effect in this case yields ferromagnetic order in the graphene substrate. We derive the band structure in the vicinity of the K points for both configurations, the Bloch wave functions and their spin polarization.

DOI: 10.1103/PhysRevB.94.235407

I. INTRODUCTION

Graphene-like two-dimensional structures have captured the imagination of experimentalists for practical applications because of the high hole/electron densities (10^{13} cm^{-2} much larger than GaAs electron gas) achieved by gating [1] at a small fraction of the cost and complexity of producing a two-dimensional electron gas with well-known semiconductor technologies. One can also build semiconductors from graphene by breaking the sublattice A/B symmetry, in systems such as boron nitride [2], generating a gap (∼5 eV) at the K point with a quadratic dispersion. Because it is undesirable to introduce substitutional impurities to modify graphene's properties, due to the rapid degradation of electron mobilities, one can resort to proximity effects [3] in order for graphene to inherit potentially useful couplings and properties such as a strong spin-orbit coupling [4], magnetism [5], and even chirality [6]. Deposited transition metals such as Co and Ni have matching lattice constants and a few layers easily form on graphene with a large perpendicular magnetic anisotropy [7]. Such magnetic layers can be used to introduce new effective couplings between graphene p_z orbitals, thus inducing a strong Rashba-type coupling, inherited from the Co/Ni overlayer, and also an electron spin polarization with perturbative modifications of the electron mobility.

In this article we consider tight-binding modeling of Co/Ni on planar graphene in two configurations. As found by DFT calculations [8], the lowest-energy configuration corresponds to one sublattice site of the graphene atop a Co/Ni atom while the neighboring sublattice atom is in a Co/Ni HCP site. For this configuration, Ref. [8] has shown that the graphene inherits an antiferromagnetic order due mostly to the sublattice asymmetry of the coupling between p_z orbitals of carbon and Co. This type of order lends itself to enhanced RKKY interactions between Co islands on graphene [9], that can be tuned to be either ferro or antiferro by gate control.

The second configuration we consider corresponds to a global lattice shift from the previous one where all graphene carbon sites fall at HCP sites of the Co/Ni layer. Referring to the detailed DFT study of Ref. [8] we will first derive the tight-binding model for the first configuration by describing the orbital overlaps and chemical potentials. We then use such parametrization to estimate the corresponding ones from the second configuration. While the first configuration yields antiferro order on graphene, the second configuration is symmetric between A/B sublattices and yields ferromagnetic order in the graphene plane.

The summary of this paper is as follows. In Sec. II we describe the two different registers we consider for the tight-binding model. Focusing first on the ATOP configuration we identify the most salient overlaps involved between the carbon $2p_z$ orbitals and the $3d$ orbitals of Co/Ni (considering only nearest-neighbor overlaps), and derive using the band folding scheme, the effective Hamiltonian for π electrons of graphene in the presence of the magnetic overlayer. Next, we shift the lattice register and consider the HCP configuration, where now the configuration is such that nondiagonal pseudospin terms arise, coupling A and B sublattices. In Sec. III we obtain the Bloch Hamiltonians for both configurations and determine the band structure and wave functions for the bulk samples. The new HCP configuration displays a nontrivial ferromagnetic ordering and a spin-dependent kinetic term proportional to the spin-splitting energy of the Co/Ni covering. Finally, we discuss spin-related properties of the new Hamiltonians for biased and equilibrium current setups.

II. ATOP AND HCP CONFIGURATIONS AND BAND FOLDING

Our system consists of a monolayer of Co atoms adsorbed on graphene. A bilayer of Co was shown to be stable [8] sustaining a strong anisotropy with magnetization per atom close

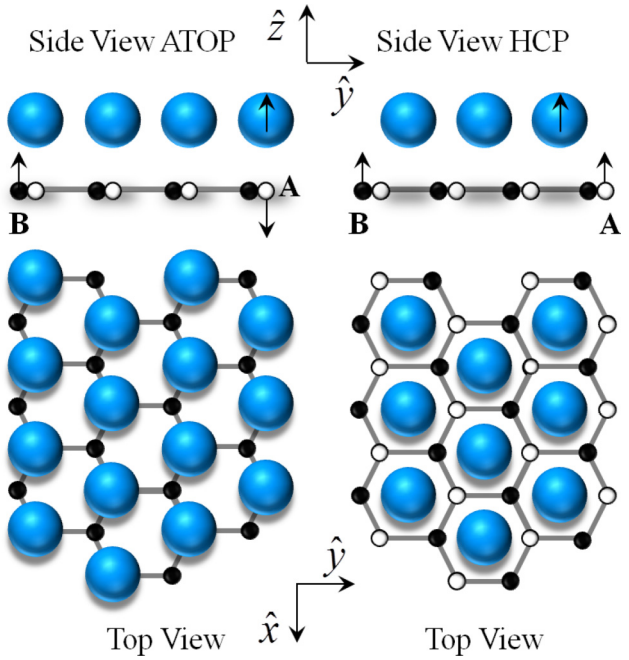

FIG. 1. Schematic picture of the configurations of a Co monolayer adsorbed on graphene. (Left) ATOP configuration: Co atoms are directly over the atoms of sublattice A and atoms of the sublattice B are in the hcp sites. (Right) HCP configuration: atoms of the sublattices A and B are at hcp sites. In both cases the magnetic order of cobalt, as well as the resulting magnetic order of the sublattices A and B, is indicated.

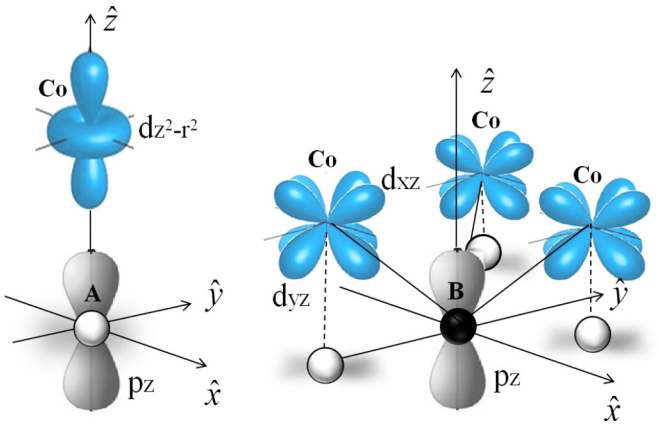

FIG. 2. Positions of the Co first neighbor around A (left) and B (right), for the ATOP configuration. The orbitals that intervene in the overlaps of Co with A and B are drawn in each case.

to the bulk values. For the model derived here, we only take into account graphene interactions with the first adsorbed layer. We consider two registries for the positions of the Co atoms with respect to graphene atoms belonging to the sublattices A and B, which are shown in Fig. 1. In the configuration of Fig. 1 (left) (ATOP configuration), the C atoms of the sublattice A are directly under the Co atoms, while atoms of sublattice B are at the HCP sites of the cobalt lattice. In the configuration of Fig. 1 (right) (HCP configuration), both sublattice atoms are at HCP sites of Co. In the model computations, the first-neighbor approximation is used. We will consider that Co is magnetized in the positive $\hat{z}$ direction (see Fig. 1). The intrinsic spin-orbit interaction (SOI) and the Rashba coupling will not be addressed here since further overlaps will be involved beyond the d orbitals of the Co. Nevertheless, in the absence of magnetism, the SOI is the only coupling generating spin effects and should be taken into account for interface metals such as Pb [10] and Au [4] to assess, e.g., the enhancement of topological properties of graphene. The SOI due to changes in the hybridization of carbon in graphene as a result of deformations of the surface due to corrugation or hydrogenation [11] will be left to future work.

A. ATOP configuration

In the ATOP configuration, as shown in the left of Fig. 2, the orbital p_z of a C atom A, Ap_z, has greatest overlap with the orbital $d_{z^2-r^2}$ (in short d_{z^2}), of the Co layer. For the neighboring B atom [see Fig. 2 (right)], the orbital p_z, Bp_z, overlaps preferentially with the orbitals d_{xz} and d_{yz} of the first-neighbor Co atoms (there are three Co atoms around each B atom of graphene). The graphene-Co coupled Hamiltonian for the ATOP configuration is the following:

$$H_{\mathrm{ATOP}} = \begin{array}{c|cc|cc} & Ap_z & Bp_z & d_{z^2-r^2} & d_{xz} \quad d_{yz} \\ \hline Ap_z & \varepsilon_p & V_{pp\pi} & V_{pdz} & 0 \quad 0 \\ Bp_z & V^*_{pp\pi} & \varepsilon_p & 0 & \hat{n}_x\widetilde{V}_{pd\pi} \quad \hat{n}_y\widetilde{V}_{pd\pi} \\ \hline d_{z^2-r^2} & -V_{pdz} & 0 & \varepsilon_{dz^2}+\delta_1 S_z & 0 \quad 0 \\ d_{xz} & 0 & -\hat{n}_x\widetilde{V}_{pd\pi} & 0 & \varepsilon_{dxz}+\delta_2 S_z \quad 0 \\ d_{yz} & 0 & -\hat{n}_y\widetilde{V}_{pd\pi} & 0 & 0 \quad \varepsilon_{dyz}+\delta_2 S_z \end{array}. \tag{1}$$

where the array consists of four subspaces. The upper left subspace contains the bare p_z-orbital site energies of graphene ε_p, and the off-diagonal overlaps $V_{pp\pi}$, between A-B sites. The upper right subspace contains the overlaps between the orbitals Ap_z and Bp_z with the orbitals d_{z^2}, d_{xz}, and d_{yz}, which are V_{pdz}, $\hat{n}_x\widetilde{V}_{pd\pi}$, and $\hat{n}_y\widetilde{V}_{pd\pi}$ (computed below), respectively, where $\hat{n}_x$, $\hat{n}_y$ are the corresponding direction cosines in a Slater-Koster construction [12,13]. Note that the lower left submatrix is the negative of the upper right submatrix since $\langle l'|H|l\rangle = (-1)^{l+l'}\langle l|H|l'\rangle$ (see Ref. [13]), where l is the orbital angular momentum quantum number ($l = 1$ for p and $l = 2$ for d orbitals).

Finally, the lower right subspace contains, in the diagonal, the energies of the coupled d orbitals, ε_{z^2}, ε_{xz}, and ε_{yz}. As we

are considering that Co is magnetized in the $\hat{z}$ direction, we add to the d-orbital energies the Stoner exchange splittings δ_1 for the orbital d_{z^2} and δ_2 for the orbitals d_{xz} and d_{yz}. We assume that d_{xz} and d_{yz} have the same exchange coupling. S_z is the z component Pauli matrix.

The overlaps between orbitals p_z, d_{xz}, and d_{yz}, are calculated using the relations [12,13]

$$\begin{aligned}\langle Bp_z|H_1|d_{xz}\rangle &= \sqrt{3}n_z^2 n_x V_{pd\sigma} + n_x\left(1-2n_z^2\right)V_{pd\pi},\\ \langle Bp_z|H_1|d_{yz}\rangle &= \sqrt{3}n_z^2 n_y V_{pd\sigma} + n_y\left(1-2n_z^2\right)V_{pd\pi},\end{aligned} \tag{2}$$

where n_x, n_y, and n_z are the direction cosines. Both overlaps have a common factor that only depends on n_z, $V_{pd\sigma}$, and $V_{pd\pi}$. In spherical coordinates $n_z = \cos\phi$, where ϕ is the polar angle. The first three neighbors, B, of the ATOP site share the same ϕ angle. Replacing $n_x = \cos\theta\sin\phi$ and $n_y = \sin\theta\sin\phi$, where θ is the azimuthal angle in the graphene plane and defining

$$\widetilde{V}_{pd\pi} = \sin\phi[\sqrt{3}n_z^2 V_{pd\sigma} + \left(1-2n_z^2\right)V_{pd\pi}], \tag{3}$$

which is a common term for both overlaps, we have

$$\begin{aligned}\langle Bp_z|H_1|d_{xz}\rangle &= \hat{n}_x\widetilde{V}_{pd\pi},\\ \langle Bp_z|H_1|d_{yz}\rangle &= \hat{n}_y\widetilde{V}_{pd\pi},\end{aligned} \tag{4}$$

where $\hat{n}_x = \cos\theta$ and $\hat{n}_y = \sin\theta$.

The eigenvalue equation for Eq. (1) has the form

$$\begin{pmatrix} H_\gamma & T\\ T^\dagger & H_\chi\end{pmatrix}\begin{pmatrix}\gamma\\ \chi\end{pmatrix} = E\begin{pmatrix}\gamma\\ \chi\end{pmatrix}, \tag{5}$$

with

$$H_\gamma = \begin{pmatrix} 0 & V_{pp\pi}\\ V_{pp\pi}^* & 0\end{pmatrix}; T = \begin{pmatrix} V_{pdz} & 0 & 0\\ 0 & \hat{n}_x\widetilde{V}_{pd\pi} & \hat{n}_y\widetilde{V}_{pd\pi}\end{pmatrix},$$

$$H_\chi = \begin{pmatrix} (\varepsilon_{dz^2}+\delta_1 S_z)-\varepsilon_p & 0 & 0\\ 0 & (\varepsilon_{dxz}+\delta_2 S_z)-\varepsilon_p & 0\\ 0 & 0 & (\varepsilon_{dyz}+\delta_2 S_z)-\varepsilon_p\end{pmatrix},$$

where we have taken the energy of the orbital p_z of graphene as the reference of zero energy, subtracting ε_p to the diagonals of H_γ and H_χ. The wave-function subspaces $\gamma = (\psi_{Ap_z}, \psi_{Bp_z})$ and $\chi = (\psi_{z^2-r^2}, \psi_{xz}, \psi_{yz})$ are coupled by T. Eliminating the wave-function subspace of the Co overlayer (χ) one arrives at

$$[H_\gamma + T(E-H_\chi)^{-1}T^\dagger]\gamma = E\gamma, \tag{6}$$

where we have folded all the information about the couplings and the Co Hamiltonian into a graphene effective coupling between A and B sublattices and renormalized the site energies. To linear order in E and lowest order in the coupling T, we can expand the inverse operator so that we obtain

$$\left[H_\gamma - TH_\chi^{-1}T^\dagger\right]\gamma \approx ES\gamma, \tag{7}$$

where $S = 1 + TH_\chi^{-2}T^\dagger$. Now one defines $\Phi = S^{1/2}\gamma$, a function that is normalized $|\Phi|^2 \approx \gamma^\dagger\gamma + \chi^\dagger\chi$ to the same order as the new effective Hamiltonian (following Ref. [14]). The final expression is then

$$S^{-1/2}\left[H_\gamma - TH_\chi^{-1}T^\dagger\right]S^{-1/2}\Phi \approx E\Phi. \tag{8}$$

The effective Hamiltonian for graphene accounting for its interactions with Co is

$$H_{\text{eff}} = S^{-1/2}\left[H_\gamma - TH_\chi^{-1}T^\dagger\right]S^{-1/2}. \tag{9}$$

The inverse of the matrix H_χ is then

$$H_\chi^{-1} = \begin{pmatrix} -\frac{(\varepsilon_p-\varepsilon_d)+\delta_1 S_z}{(\varepsilon_p-\varepsilon_d)^2-\delta_1^2} & 0 & 0\\ 0 & -\frac{(\varepsilon_p-\varepsilon_d)+\delta_2 S_z}{(\varepsilon_p-\varepsilon_d)^2-\delta_2^2} & 0\\ 0 & 0 & -\frac{(\varepsilon_p-\varepsilon_d)+\delta_2 S_z}{(\varepsilon_p-\varepsilon_d)^2-\delta_2^2}\end{pmatrix}, \tag{10}$$

so the product $TH_\chi^{-1}T^\dagger$ is expanded as

$$TH_\chi^{-1}T^\dagger = \begin{pmatrix} V_{pdz} & 0 & 0\\ 0 & \hat{n}_{mx}\widetilde{V}_{pd\pi} & \hat{n}_{my}\widetilde{V}_{pd\pi}\end{pmatrix}\begin{pmatrix} -\frac{(\varepsilon_p-\varepsilon_d)+\delta_1 S_z}{(\varepsilon_p-\varepsilon_d)^2-\delta_1^2} & 0 & 0\\ 0 & -\frac{(\varepsilon_p-\varepsilon_d)+\delta_2 S_z}{(\varepsilon_p-\varepsilon_d)^2-\delta_2^2} & 0\\ 0 & 0 & -\frac{(\varepsilon_p-\varepsilon_d)+\delta_2 S_z}{(\varepsilon_p-\varepsilon_d)^2-\delta_2^2}\end{pmatrix}\begin{pmatrix} -V_{pdz} & 0\\ 0 & -\hat{n}_{mx}\widetilde{V}_{pd\pi}\\ 0 & -\hat{n}_{my}\widetilde{V}_{pd\pi}\end{pmatrix},$$

where we have included the subindex m to the cosine directors n_{mx}, n_{my} to indicate that for each of the three Co atoms surrounding a B-type atom on graphene (see Fig. 2), we have a different overlap. The product becomes the simple diagonal expression

$$TH_\chi^{-1}T^\dagger = \begin{pmatrix} \frac{(\varepsilon_p-\varepsilon_d)+\delta_1 S_z}{(\varepsilon_p-\varepsilon_d)^2-\delta_1^2}V_{pdz}^2 & 0\\ 0 & \frac{(\varepsilon_p-\varepsilon_d)+\delta_2 S_z}{(\varepsilon_p-\varepsilon_d)^2-\delta_2^2}\widetilde{V}_{pd\pi}^2\left[\hat{n}_{mx}^2+\hat{n}_{my}^2\right]\end{pmatrix}. \tag{11}$$

The Hamiltonian for the ATOP configuration is obtained substituting Eq. (11) into Eq. (9), approximating $S \sim \mathbb{1}$ and performing the sum $\sum_{m=1}^{3}[n_{mx}^2 + n_{my}^2] = 3$, which accounts for the contribution to the site energy due to hops of electrons that go from B to Co and return back to B (see Ref. [15]). The effective Hamiltonian is then

$$H_{\text{ATOP}} \approx H_\gamma - \begin{pmatrix} \frac{(\varepsilon_p-\varepsilon_d)+\delta_1 S_z}{(\varepsilon_p-\varepsilon_d)^2-\delta_1^2}V_{pdz}^2 & 0\\ 0 & 3\frac{(\varepsilon_p-\varepsilon_d)+\delta_2 S_z}{(\varepsilon_p-\varepsilon_d)^2-\delta_2^2}\widetilde{V}_{pd\pi}^2\end{pmatrix}. \tag{12}$$

In second quantized form, the Hamiltonian for the full Brillouin zone can be written as

$$H_{\mathrm{ATOP}} = -\sum_{\langle ij\rangle} \gamma_0 a_i^\dagger b_j - \frac{(\varepsilon_p-\varepsilon_d)+\delta_1 S_z}{(\varepsilon_p-\varepsilon_d)^2-\delta_1^2} V_{pdz}^2 \sum_i a_i^\dagger a_i - 3\frac{(\varepsilon_p-\varepsilon_d)+\delta_2 S_z}{(\varepsilon_p-\varepsilon_d)^2-\delta_2^2} \widetilde{V}_{pd\pi}^2 \sum_j b_j^\dagger b_j, \tag{13}$$

where $\gamma_0 = -V_{pp\pi}$ is the regular off-diagonal kinetic term in graphene and a_i and b_j are the annihilation operators in the sites A and B graphene sublattices.

B. HCP configuration

For the lattice symmetric or HCP configuration, the orbital d_{z^2} does not intervene as in the previous case due to the relative positions of the Co and graphene atoms, as all graphene sites now see the Co/Ni as the B sites in the ATOP configuration. The overlap matrix is given by

$$\begin{bmatrix} \begin{matrix} Ap_z & Bp_z \end{matrix} & \begin{matrix} d_{z^2-r^2} & d_{xz} & d_{yz} \end{matrix} \\ \begin{bmatrix} \varepsilon_p & V_{pp\pi} \\ V_{pp\pi}^* & \varepsilon_p \end{bmatrix} & \begin{bmatrix} 0 & \hat{n}_x\widetilde{V}_{pd\pi} & \hat{n}_y\widetilde{V}_{pd\pi} \\ 0 & \hat{n}_x\widetilde{V}_{pd\pi} & \hat{n}_y\widetilde{V}_{pd\pi} \end{bmatrix} \\ \begin{bmatrix} 0 & 0 \\ -\hat{n}_x\widetilde{V}_{pd\pi} & -\hat{n}_x\widetilde{V}_{pd\pi} \\ -\hat{n}_y\widetilde{V}_{pd\pi} & -\hat{n}_y\widetilde{V}_{pd\pi} \end{bmatrix} & \begin{bmatrix} \varepsilon_{dz^2}+\delta_1 S_z & 0 & 0 \\ 0 & \varepsilon_{dxz}+\delta_2 S_z & 0 \\ 0 & 0 & \varepsilon_{dyz}+\delta_2 S_z \end{bmatrix} \end{bmatrix}. \tag{14}$$

In this case A and B see the same environment of three Co atoms at the same distance, as can be seen in Fig. 3. Both graphene sites interact with them through the orbitals d_{xz} and d_{yz}.

The product $T H_\chi^{-1} T^\dagger$ is now

$$T H_\chi^{-1} T^\dagger = \begin{pmatrix} 0 & \hat{n}_{lx}\widetilde{V}_{pd\pi} & \hat{n}_{ly}\widetilde{V}_{pd\pi} \\ 0 & \hat{n}_{lmx}\widetilde{V}_{pd\pi} & \hat{n}_{lmy}\widetilde{V}_{pd\pi} \end{pmatrix} \begin{pmatrix} -\frac{(\varepsilon_p-\varepsilon_d)+\delta_1 S_z}{(\varepsilon_p-\varepsilon_d)^2-\delta_1^2} & 0 & 0 \\ 0 & -\frac{(\varepsilon_p-\varepsilon_d)+\delta_2 S_z}{(\varepsilon_p-\varepsilon_d)^2-\delta_2^2} & 0 \\ 0 & 0 & -\frac{(\varepsilon_p-\varepsilon_d)+\delta_2 S_z}{(\varepsilon_p-\varepsilon_d)^2-\delta_2^2} \end{pmatrix} \begin{pmatrix} 0 & 0 \\ -\hat{n}_{lx}\widetilde{V}_{pd\pi} & -\hat{n}_{lmx}\widetilde{V}_{pd\pi} \\ -\hat{n}_{ly}\widetilde{V}_{pd\pi} & -\hat{n}_{lmy}\widetilde{V}_{pd\pi} \end{pmatrix},$$

where, as before, $\hat{n}_l$ denote direction cosines in the plane that go from the site A to the Co $l = 1,2,3$ (A-Co direction) and $\hat{n}_{lm}$ are direction cosines in the plane that go from the site B to the Co $l = 1,2,3$ (B-Co direction) (see Fig. 4). Performing the product we have:

$$T H_\chi^{-1} T^\dagger = \begin{pmatrix} \frac{(\varepsilon_p-\varepsilon_d)+\delta_2 S_z}{(\varepsilon_p-\varepsilon_d)^2-\delta_2^2}\widetilde{V}_{pd\pi}^2\left[\hat{n}_{lx}^2+\hat{n}_{ly}^2\right] & \frac{(\varepsilon_p-\varepsilon_d)+\delta_2 S_z}{(\varepsilon_p-\varepsilon_d)^2-\delta_2^2}\widetilde{V}_{pd\pi}^2\left[\hat{n}_{lx}\hat{n}_{lmx}+\hat{n}_{ly}\hat{n}_{lmy}\right] \\ \frac{(\varepsilon_p-\varepsilon_d)+\delta_2 S_z}{(\varepsilon_p-\varepsilon_d)^2-\delta_2^2}\widetilde{V}_{pd\pi}^2[\hat{n}_{lx}\hat{n}_{lmx}+\hat{n}_{ly}\hat{n}_{lmy}] & \frac{(\varepsilon_p-\varepsilon_d)+\delta_2 S_z}{(\varepsilon_p-\varepsilon_d)^2-\delta_2^2}\widetilde{V}_{pd\pi}^2\left[\hat{n}_{lmx}^2+\hat{n}_{lmy}^2\right] \end{pmatrix}. \tag{15}$$

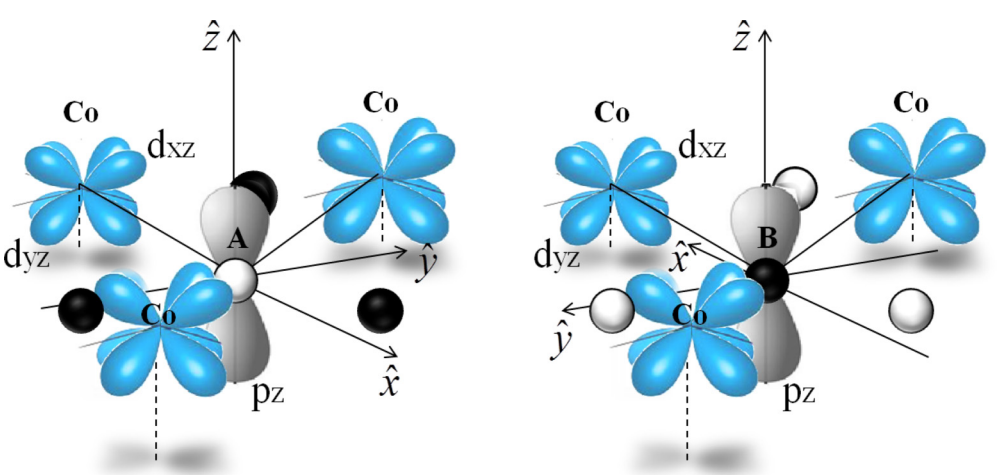

FIG. 3. Positions of the Co first neighbor around A (left) and B (right), for the HCP configuration. The orbitals that intervene in the overlaps of Co with A and B are drawn in each case.

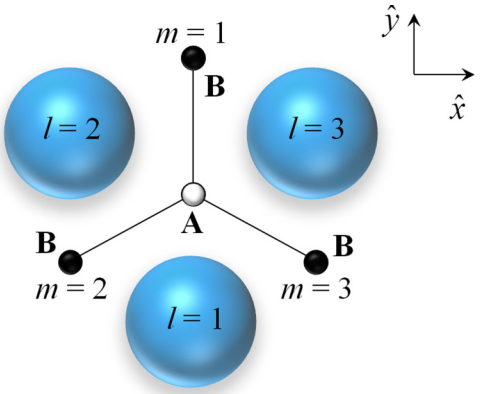

FIG. 4. Positions of the Co and B carbon atoms around a carbon atom A, in the HCP configuration of Co/graphene. $l = 1,2,3$ represents the Co surrounding A, and $m = 1,2,3$ represents the hops from A to B.

The Hamiltonian for the symmetric configuration is obtained substituting Eq. (15) into Eq. (9), and that $\sum_{l=1}^{3}[n_{lx}^2 + n_{ly}^2] = 3$, which accounts for the contribution to the site energy of hops of electrons that go from A to Co and return back to A. $\sum_{m,l=1}^{3}[n_{lmx}^2 + n_{lmy}^2] = 3$ given that $n_{lmx} = \cos\theta'$ and $n_{lmy} = \sin\theta'$, where θ' is the azimuthal angle for the overlap between site B and the Co orbitals. The latter sum accounts for the contribution to the site energy of hops of electrons that go from B to Co and return back to B.

Finally, we have the somewhat more complicated summation $\sum_{m,l=1}^{3}[\hat{n}_{lx}\hat{n}_{lmx} + \hat{n}_{ly}\hat{n}_{lmy}]$, which is performed in detail in Appendix A. The Hamiltonian for this configuration is then

$$H_{\rm HCP} \approx H_\gamma - \begin{pmatrix} 3\frac{(\varepsilon_p-\varepsilon_d)+\delta_2 S_z}{(\varepsilon_p-\varepsilon_d)^2-\delta_2^2}\widetilde{V}_{pd\pi}^2 & -\frac{(\varepsilon_p-\varepsilon_d)+\delta_2 S_z}{(\varepsilon_p-\varepsilon_d)^2-\delta_2^2}\widetilde{V}_{pd\pi}^2 \\ -\frac{(\varepsilon_p-\varepsilon_d)+\delta_2 S_z}{(\varepsilon_p-\varepsilon_d)^2-\delta_2^2}\widetilde{V}_{pd\pi}^2 & 3\frac{(\varepsilon_p-\varepsilon_d)+\delta_2 S_z}{(\varepsilon_p-\varepsilon_d)^2-\delta_2^2}\widetilde{V}_{pd\pi}^2 \end{pmatrix}. \tag{16}$$

The complete HCP Hamiltonian, in terms of the creation and annihilation operators in the sites A and B of graphene, a_i and b_j, is given by

$$H_{\rm HCP} = \left(-\gamma_0 + \frac{(\varepsilon_p-\varepsilon_d)+\delta_2 S_z}{(\varepsilon_p-\varepsilon_d)^2-\delta_2^2}\widetilde{V}_{pd\pi}^2\right)\sum_{\langle ij\rangle} a_i^\dagger b_j - 3\frac{(\varepsilon_p-\varepsilon_d)+\delta_2 S_z}{(\varepsilon_p-\varepsilon_d)^2-\delta_2^2}\widetilde{V}_{pd\pi}^2\left(\sum_i a_i^\dagger a_i + \sum_j b_j^\dagger b_j\right). \tag{17}$$

III. BAND STRUCTURE AND MAGNETIC ORDER OF THE COBALT/GRAPHENE SYSTEM

We now derive the Hamiltonians in reciprocal space in order to determine the band structures of graphene modified by adsorbed and polarized Co/Ni in both ATOP and HCP configurations. The Bloch Hamiltonian is derived by computing the following matrix elements in pseudospin space

$$H_{\rm AA}(\mathbf{k}) = \frac{1}{N}\sum_{l=1}^{N}\sum_{j=1}^{N} e^{i\mathbf{k}\cdot(\mathbf{R}_{Aj}-\mathbf{R}_{Al})}\langle\phi_{Al}|H|\phi_{Aj}\rangle = H_{\rm BB}(\mathbf{k}), \tag{18}$$

where N is the number of unit cells, $\mathbf{k}$ is the Bloch wave vector and we take $(\mathbf{R}_{Aj} - \mathbf{R}_{Al}) = 0$ since we do not consider second-neighbor interactions (only $j = l$ terms). The off-diagonal terms in pseudospin space are

$$H_{\rm AB}(\mathbf{k}) = \frac{1}{N}\sum_{l=1}^{N}\sum_{j=1}^{N} e^{i\mathbf{k}\cdot(\mathbf{R}_{Bj}-\mathbf{R}_{Al})}\langle\phi_{Al}|H|\phi_{Bj}\rangle = H_{\rm BA}^\dagger(\mathbf{k}), \tag{19}$$

where $(\mathbf{R}_{Bj} - \mathbf{R}_{Al}) = \Delta_m$ is restricted to nearest neighbors with $m = 1,2,3$ and $\Delta_1 = (0, a/\sqrt{3})$ $\Delta_2 = (a/2, -a/2\sqrt{3})$, $\Delta_3 = (-a/2, -a/2\sqrt{3})$ (see Fig. 1).

For matrix element $H_{\rm AA}$, we consider couplings that connect A to a Co/Ni orbital and then return to same A site (corrections to the site energy see Ref. [15]). In $H_{\rm AB}$, we consider couplings that connect A to Co/Ni sites and then go to one of the three B atoms that are nearest neighbors (corrections to the nearest-neighbor matrix elements). In the following we will compute these matrix elements and derive the resulting band structure in the vicinity of the K points.

A. ATOP Bands

Using Eqs. (18) and (19), and evaluating in the vicinity of the K points $K_\xi = \xi[(4\pi/3a), 0]$, the continuum Hamiltonian in reciprocal space for the ATOP configuration can be shown to be

$$H_{\rm ATOP}(\mathbf{k}) = \begin{pmatrix} -\frac{(\varepsilon_p-\varepsilon_d)+\delta_1}{(\varepsilon_p-\varepsilon_d)^2-\delta_1^2}V_{pdz}^2 & v(\xi p_x - i p_y) & 0 & 0 \\ v(\xi p_x + i p_y) & -\frac{(\varepsilon_p-\varepsilon_d)-\delta_1}{(\varepsilon_p-\varepsilon_d)^2-\delta_1^2}V_{pdz}^2 & 0 & 0 \\ 0 & 0 & -3\frac{(\varepsilon_p-\varepsilon_d)+\delta_2}{(\varepsilon_p-\varepsilon_d)^2-\delta_2^2}\widetilde{V}_{pd\pi}^2 & v(\xi p_x - i p_y) \\ 0 & 0 & v(\xi p_x + i p_y) & -3\frac{(\varepsilon_p-\varepsilon_d)-\delta_2}{(\varepsilon_p-\varepsilon_d)^2-\delta_2^2}\widetilde{V}_{pd\pi}^2 \end{pmatrix}. \tag{20}$$

With a more compact parametrization

$$H_{\mathrm{ATOP}}(\mathbf{k}) = \begin{pmatrix} \mu - h_{0z} - \frac{h_{z0}}{2} - \frac{h_{zz}}{2} & v(\xi p_x - i p_y) & 0 & 0 \\ v(\xi p_x + i p_y) & \mu - h_{0z} + \frac{h_{z0}}{2} + \frac{h_{zz}}{2} & 0 & 0 \\ 0 & 0 & \mu + h_{0z} - \frac{h_{z0}}{2} + \frac{h_{zz}}{2} & v(\xi p_x - i p_y) \\ 0 & 0 & v(\xi p_x + i p_y) & \mu + h_{0z} + \frac{h_{z0}}{2} - \frac{h_{zz}}{2} \end{pmatrix}, \tag{21}$$

where $\mu = -0.622$ eV, $h_{0z} = 0.195$ eV, $h_{z0} = -0.214$ eV, and $h_{zz} = -0.766$ eV, are coefficients determined by *ab initio* calculations, in the vicinity of the K points, in Ref. [8]. Comparing Eqs. (20) and (21), we can make the identification:

$$\begin{aligned} -\frac{V_{pdz}^2(\varepsilon_p - \varepsilon_d)}{(\varepsilon_p - \varepsilon_d)^2 - \delta_1^2} &= \mu - h_{0z}, \quad \frac{\delta_1 V_{pdz}^2}{(\varepsilon_p - \varepsilon_d)^2 - \delta_1^2} = \frac{(h_{z0} + h_{zz})}{2}, \\ -3\frac{\widetilde{V}_{pd\pi}^2(\varepsilon_p - \varepsilon_d)}{(\varepsilon_p - \varepsilon_d)^2 - \delta_2^2} &= \mu + h_{0z}, \quad 3\frac{\delta_2 \widetilde{V}_{pd\pi}^2}{(\varepsilon_p - \varepsilon_d)^2 - \delta_2^2} = \frac{(h_{z0} - h_{zz})}{2}. \end{aligned} \tag{22}$$

The identification allows us to determine the coefficients of the Hamiltonian for configurations ATOP and later estimate the parameters of model HCP. In the Appendix we explicitly write the coefficients h_{0z},h_{z0},h_{zz}, and μ in terms of the Slater-Koster coefficients.

In Eq. (20) $v = \sqrt{3}a\gamma_0/(2\hbar)$, with $-\gamma_0 = V_{pp\pi} = -3.033$ eV. Diagonalization of the Hamiltonian in Eq. (21) gives the valence and conduction bands

$$\begin{aligned} \epsilon_v(\mathbf{k}) &= \tfrac{1}{2}\left(2\mu - s_z h_{z0} - \sqrt{(2h_{0z} + s_z h_{zz})^2 + 4v^2\hbar^2|\mathbf{k}|^2}\right), \\ \epsilon_c(\mathbf{k}) &= \tfrac{1}{2}\left(2\mu - s_z h_{z0} + \sqrt{(2h_{0z} + s_z h_{zz})^2 + 4v^2\hbar^2|\mathbf{k}|^2}\right). \end{aligned} \tag{23}$$

where $s_z = \pm 1$ corresponding to the two spin eigenvalues. As a consequence of the A-B asymmetry due to the ATOP geometry, there is a mass term $m_v = (2h_{0z} + s_z h_{zz})/2v$ that will generate spin-dependent gaps [16,17] and a quadratic dispersion (see Fig. 5). Depending on the material overlaps we can have a light spin-up holes and heavier spin-down holes. On the other hand, for the conduction band it is the up-spin electrons that are lighter in relation to their down-spin counterparts. Something that would be more difficult to assess form DFT studies, that is clear from the analytical picture, is that an interplay between pseudospin and spin-active components of the Hamiltonian controls the spin-dependent effective masses, which may have a high contrast making one spin species much more mobile

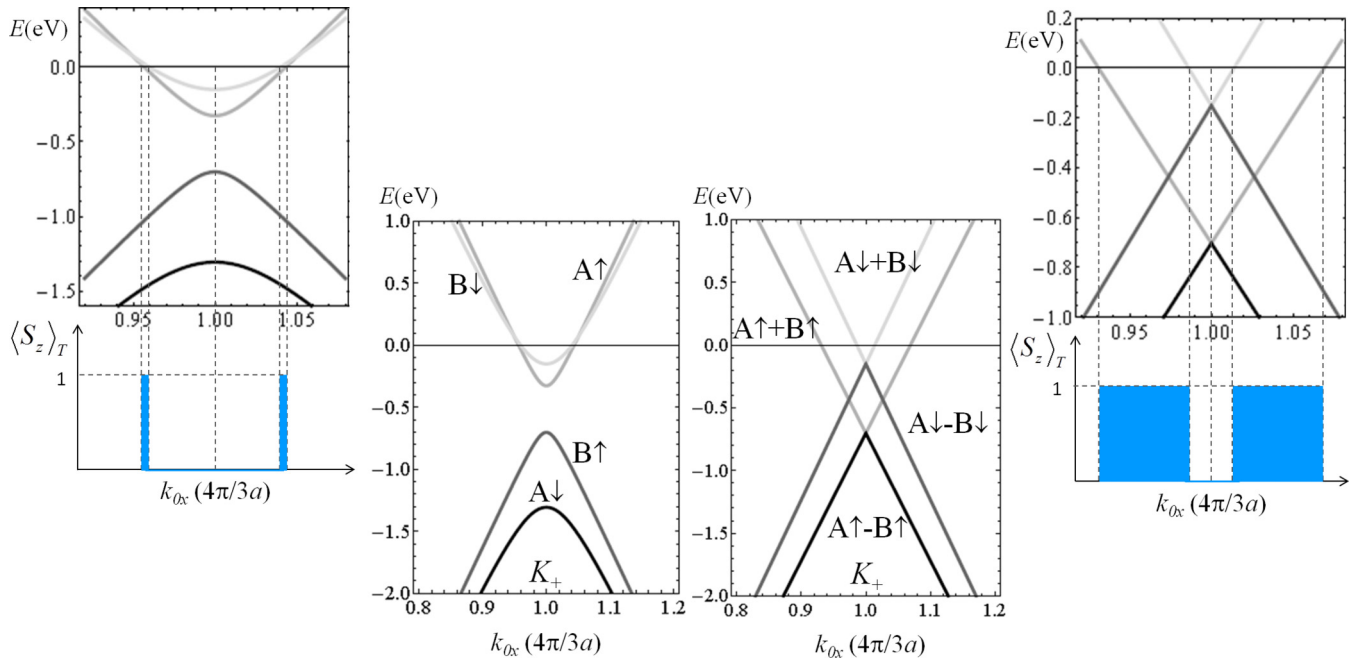

FIG. 5. Band structure in the vicinity of the Dirac point for a monolayer of Co over graphene in the ATOP configuration (center left) and the HCP configuration (center right). The Fermi level (zero of energy) is indicated in both plots with a continuous line. In both cases the graphene layer is n doped [17]. The eigenvectors corresponding to each band are indicated for both configurations. k_{0x} is the adimensional wave vector in the $\hat{x}$ direction. In this plot $p_y = 0$, $p_x = \hbar k_x - \hbar K_\xi$, and $\xi = +1$. The behavior of the total magnetization of graphene $\langle S_z\rangle_T$, given by the contribution of all bands, as a function of the wave vector $k_x = k_{0x}(4\pi/3a)$, for the ATOP configuration (top left) and the HCP configuration (top right). The shaded regions (blue) indicate the zones in which the spin polarization is different from zero.

than the other. Thus, the ATOP configuration modifies the linear dispersion in a qualitative way changing the dispersion and mobility of the pristine graphene layer.

For $\mathbf{k}=0$, this Hamiltonian $H_{\mathrm{ATOP}}(\mathbf{k})$ is diagonal in the basis

$$\begin{pmatrix} A\uparrow \\ A\downarrow \\ B\uparrow \\ B\downarrow \end{pmatrix} = \begin{pmatrix} 1 \\ 0 \\ 0 \\ 0 \end{pmatrix}, \begin{pmatrix} 0 \\ 1 \\ 0 \\ 0 \end{pmatrix}, \begin{pmatrix} 0 \\ 0 \\ 1 \\ 0 \end{pmatrix}, \begin{pmatrix} 0 \\ 0 \\ 0 \\ 1 \end{pmatrix}. \tag{24}$$

Under this condition, we can write:

$$H_{\mathrm{ATOP}}(\mathbf{k}=0) = \mu \mathbb{1}_\sigma \mathbb{1}_s - h_{0z}\sigma_z \mathbb{1}_s - \frac{h_{z0}}{2}\mathbb{1}_\sigma S_z - \frac{h_{zz}}{2}\sigma_z S_z, \tag{25}$$

where $\mathbb{1}_s$ and $\mathbb{1}_\sigma$ are the identity matrices in the spin and pseudospin space respectively.

Looking at Eq. (25), we can easily recognize the effect of each term on the energy of the system. The first term represents a global energy shift, which is given by the chemical potential $\mu = -0.622$ eV. The negative sign indicates that electrons are transferred from Co to graphene. This electron transfer is depicted in Fig. 5 (left), where the bare graphene bands are shifted by μ.

The second term is a sublattice antisymmetric site energy, $h_{0z} = 0.195$ eV. The site energy, in this case, decreases in sublattice A and increases in B, indicating that the sublattice A is more strongly influenced by Co than B (see Figs. 1 and 2), due to the p_z-d_{z^2} overlap of sublattice A.

The third term is a sublattice symmetric spin-dependent coupling between Co and graphene. This term gives the spin coupling averaged over sublattices A and B. We have $h_{z0}/2 = -0.107$ eV, making the states $A\downarrow$ and $B\downarrow$ energetically favorable. As we have chosen the reference spin magnetization of the Co to be up-spin, therefore, the sublattice averaged magnetic order of graphene is antiferromagnetic (AFM) (with respect to Co).

Finally, the fourth term corresponds to a sublattice antisymmetric kinetic exchange coupling between Co and graphene spins. We have $h_{zz}/2 = -0.383$ eV, which as can be seen in Eq. (25), makes the states $A\downarrow$ and $B\uparrow$ energetically favorable, indicating that sublattice A is AFM while sublattice B is FM with respect to Co spin magnetization.

Although the previous simple tight-binding model seems quite good, there are nevertheless some inconsistencies due to the truncation of higher-order terms involving more complex couplings. We have used a separate spin splitting parameter δ_2 to describe the coupling to d_{xz},d_{yz} bands. For there to be a up-spin magnetization, the average δ over all d orbitals of the Co, should be negative. This is consistent with the top-right relation [Eq. (22)] between DFT parameters [8] and tight-binding parameters. Nevertheless, the bottom-right equation implies a positive δ value since $(\varepsilon_p - \varepsilon_d)^2 > \delta_2^2$, from an estimation using Hartree-Fock orbital energies [18] and δ_2 from Ref. [8]. This cannot be corrected by including d_{xy} and $d_{x^2-y^2}$ since these contributions add up with the same sign. In the DFT calculation, the ratio between $\delta_1 \sim -2.76$ eV and $\delta_2 \sim -1.083$ eV is almost a factor of three but both have consistently a negative sign, i.e., up (majority) spin is lower energy than down (minority) spin. All the rest of the parameters of the tight binding have consistent values to DFT.

B. HCP bands

The continuum Hamiltonian in the vicinity of the K points for the HCP configuration is

$$H_{\mathrm{HCP}}(\mathbf{k}) = \begin{pmatrix} -3\frac{\varepsilon+\delta_2}{\varepsilon^2-\delta_2^2}\widetilde{V}_{pd\pi}^2 & 0 & -\frac{v}{\gamma_0}\left(-\gamma_0 + \frac{\varepsilon+\delta_2}{\varepsilon^2-\delta_2^2}\widetilde{V}_{pd\pi}^2\right)p^* & 0 \\ 0 & -3\frac{\varepsilon-\delta_2}{\varepsilon^2-\delta_2^2}\widetilde{V}_{pd\pi}^2 & 0 & -\frac{v}{\gamma_0}\left(-\gamma_0 + \frac{\varepsilon-\delta_2}{\varepsilon^2-\delta_2^2}\widetilde{V}_{pd\pi}^2\right)p^* \\ -\frac{v}{\gamma_0}\left(-\gamma_0 + \frac{\varepsilon+\delta_2}{\varepsilon^2-\delta_2^2}\widetilde{V}_{pd\pi}^2\right)p & 0 & -3\frac{\varepsilon+\delta_2}{\varepsilon^2-\delta_2^2}\widetilde{V}_{pd\pi}^2 & 0 \\ 0 & -\frac{v}{\gamma_0}\left(-\gamma_0 + \frac{\varepsilon-\delta_2}{\varepsilon^2-\delta_2^2}\widetilde{V}_{pd\pi}^2\right)p & 0 & -3\frac{\varepsilon-\delta_2}{\varepsilon^2-\delta_2^2}\widetilde{V}_{pd\pi}^2 \end{pmatrix}, \tag{26}$$

where $p = \xi p_x + i p_y$, $p^* = \xi p_x - i p_y$, and $\varepsilon = \varepsilon_p - \varepsilon_d$. This Hamiltonian can be written as:

$$H_{\mathrm{HCP}}(\mathbf{k}) = \begin{pmatrix} -\mu' - h'_{z0} & 0 & -\frac{v}{\gamma_0}(-\gamma_0 - h'_{0x} - h'_{zx})p^* & 0 \\ 0 & -\mu' + h'_{z0} & 0 & -\frac{v}{\gamma_0}(-\gamma_0 - h'_{0x} + h'_{zx})p^* \\ -\frac{v}{\gamma_0}(-\gamma_0 - h'_{0x} - h'_{zx})p & 0 & -\mu' - h'_{z0} & 0 \\ 0 & -\frac{v}{\gamma_0}(-\gamma_0 - h'_{0x} + h'_{zx})p & 0 & -\mu' + h'_{z0} \end{pmatrix}. \tag{27}$$

In order to estimate the coefficients μ', h'_{z0}, h'_{0x}, and h'_{zx}, of this Hamiltonian, we refer to the coupling of the B site in the ATOP configuration, which was parameterized by DFT. Comparing equations (22), (26), and (27) we arrive at the values

$$\mu' = -(\mu + h_{0z}) = 0.427\,\mathrm{eV}, \quad h'_{0x} = -\frac{\mu'}{3} = -0.142\,\mathrm{eV},$$
$$h'_{z0} = \frac{h_{z0} - h_{zz}}{2} = 0.276\,\mathrm{eV}, \quad h'_{zx} = -\frac{h'_{z0}}{3} = -0.092\,\mathrm{eV}. \tag{28}$$

Diagonalization of the Hamiltonian $H_{\rm HCP}(\mathbf{k})$ gives the eigenvalues

$$\begin{aligned}\epsilon_v(\mathbf{k}) &= -\mu' + s_z h'_{z0} + \frac{v\hbar}{\gamma_0}(-\gamma_0 - h'_{0x} + s_z h'_{zx})|\mathbf{k}|,\\ \epsilon_c(\mathbf{k}) &= -\mu' + s_z h'_{z0} - \frac{v\hbar}{\gamma_0}(-\gamma_0 - h'_{0x} + s_z h'_{zx})|\mathbf{k}|.\end{aligned} \tag{29}$$

where s_z are the eigenvalues of S_z and correspond to the two possible spin orientations. In contrast to the ATOP configuration, here the dispersion is linear with a modified velocity $\tilde{v}_F = v(-\gamma_0 - h'_{0x} + s_z h'_{zx})/\gamma_0$. Of course, corrections to velocities are one order of magnitude smaller that the pristine graphene values [see Eqs. (28)].

One can diagonalize the Hamiltonian $H_{\rm HCP}(\mathbf{k})$ in the basis

$$\begin{pmatrix} A\uparrow \\ A\downarrow \\ B\uparrow \\ B\downarrow \end{pmatrix} = \frac{1}{\sqrt{2}}\begin{pmatrix} 0 \\ 1 \\ 0 \\ \xi e^{i\xi\phi_k} \end{pmatrix}, \frac{1}{\sqrt{2}}\begin{pmatrix} 1 \\ 0 \\ \xi e^{i\xi\phi_k} \\ 0 \end{pmatrix}, \frac{1}{\sqrt{2}}\begin{pmatrix} 0 \\ 1 \\ 0 \\ -\xi e^{i\xi\phi_k} \end{pmatrix}, \frac{1}{\sqrt{2}}\begin{pmatrix} 1 \\ 0 \\ -\xi e^{i\xi\phi_k} \\ 0 \end{pmatrix}, \tag{30}$$

where $\phi_k = \arctan(p_y/p_x)$. Given that in Eq. (26) we have other nondiagonal terms besides the bare graphene terms, and therefore we have other $\mathbf{k}$-dependent terms, we cannot make a useful analysis at $\mathbf{k} = 0$ as in the ATOP case. The diagonal Hamiltonian for $\mathbf{k} \neq 0$ close to K_ξ is:

$$\begin{aligned} H_{\rm HCP}(\mathbf{k}) &= -\mu' \begin{pmatrix} {\scriptstyle A\uparrow+B\uparrow} & {\scriptstyle A\downarrow+B\downarrow} & {\scriptstyle A\uparrow-B\uparrow} & {\scriptstyle A\downarrow-B\downarrow} \\ 1 & 0 & 0 & 0 \\ 0 & 1 & 0 & 0 \\ 0 & 0 & 1 & 0 \\ 0 & 0 & 0 & 1 \end{pmatrix} + \frac{v\hbar}{\gamma_0}|\mathbf{k}|(h'_{0x} + \gamma_0) \begin{pmatrix} {\scriptstyle A\uparrow+B\uparrow} & {\scriptstyle A\downarrow+B\downarrow} & {\scriptstyle A\uparrow-B\uparrow} & {\scriptstyle A\downarrow-B\downarrow} \\ 1 & 0 & 0 & 0 \\ 0 & 1 & 0 & 0 \\ 0 & 0 & -1 & 0 \\ 0 & 0 & 0 & -1 \end{pmatrix} \\ &\quad - h'_{z0} \begin{pmatrix} {\scriptstyle A\uparrow+B\uparrow} & {\scriptstyle A\downarrow+B\downarrow} & {\scriptstyle A\uparrow-B\uparrow} & {\scriptstyle A\downarrow-B\downarrow} \\ 1 & 0 & 0 & 0 \\ 0 & -1 & 0 & 0 \\ 0 & 0 & 1 & 0 \\ 0 & 0 & 0 & -1 \end{pmatrix} + \frac{v\hbar}{\gamma_0}|\mathbf{k}|h'_{zx} \begin{pmatrix} {\scriptstyle A\uparrow+B\uparrow} & {\scriptstyle A\downarrow+B\downarrow} & {\scriptstyle A\uparrow-B\uparrow} & {\scriptstyle A\downarrow-B\downarrow} \\ 1 & 0 & 0 & 0 \\ 0 & -1 & 0 & 0 \\ 0 & 0 & -1 & 0 \\ 0 & 0 & 0 & 1 \end{pmatrix} \\ &= -\mu' \mathbb{1}_\sigma \mathbb{1}_s + \frac{v\hbar}{\gamma_0}|\mathbf{k}|(h'_{0x} + \gamma_0)\widetilde{\sigma}_z \mathbb{1}_s - h'_{z0}\mathbb{1}_\sigma S_z + \frac{v\hbar}{\gamma_0}|\mathbf{k}|h'_{zx}\widetilde{\sigma}_z S_z, \end{aligned} \tag{31}$$

where $\widetilde{\sigma}_z$ is the pseudospin matrix in the basis of Eq. (30). Within this basis, the interpretation of the terms is not so straightforward as for the ATOP configuration. However, one can see that the first term also shifts the site energy, with a chemical potential $\mu' = 0.427$ eV, that represents a transfer of electrons from Co/Ni to graphene. We can see this effect in Fig. 5 (right panels). For the second term we have $h'_{0x} = -0.142$ eV, and looking at Eq. (31), we see that the states $A\uparrow - B\uparrow$ and $A\downarrow - B\downarrow$ are equally favorable, indicating symmetry between the sublattices A and B. This is because in the sublattice symmetric configuration, both A and B, are at the HCP sites of Co (Figs. 1 and 3).

The magnetic order of graphene, with respect to Co magnetic order, is determined by the eigenvalue of lowest energy and its corresponding eigenvector in Eq. (31). Given that $h'_{z0} = 0.276$ eV and $h'_{zx} = -0.092$ eV, this state corresponds to $|A\uparrow - B\uparrow\rangle$. Using this state, with $k_y = 0$ and $\xi = 1$, we have

$$\begin{aligned}\langle S_z\rangle &= \langle A\uparrow - B\uparrow|\mathbb{1}_\sigma S_z|A\uparrow - B\uparrow\rangle \\ &= \frac{1}{2}\begin{pmatrix}1 & 0 & -1 & 0\end{pmatrix}\begin{pmatrix}1 & 0 & 0 & 0\\ 0 & -1 & 0 & 0\\ 0 & 0 & 1 & 0\\ 0 & 0 & 0 & -1\end{pmatrix}\begin{pmatrix}1\\ 0\\ -1\\ 0\end{pmatrix} = 1,\end{aligned} \tag{32}$$

so every band has a full spin polarization in either of the two spin orientations as depicted in right-hand panel of Fig. 5.

The coupling of the spin and kinetic energy [see last term in Eq. (31)] induces a striking behavior, which mimics a spin-orbit coupling induced by the bias current and the magnetism of the Co. In the sense of equilibrium/persistent currents [19], at $k = 0$ all bands have occupation below the Fermi energy, thus the spin polarization is zero at both K points. As k_x increases, e.g., in the positive direction, (see Fig. 5 top-right panel) one of the bands emerges above the Fermi level and we have a net polarization, which is up spin. A range of k_x values preserves this polarization until a second band emerges from the Fermi sea, then the polarization returns to zero. The same behavior occurs in the opposite k_x direction. This behavior is also borne out from the ATOP configuration but within a smaller wave-vector range (see Fig. 5 top-left panel) in the vicinity of the K point. Note that this term is not derived from the atomic SOI (as is the case for both the intrinsic and Rashba interactions) but is purely parameterized by the spin-splitting energy of the Co and the wave-vector deviation from the K point. As can be seen from Eqs. (22) and (28), if the spin-splitting energy $\delta_{1,2}$ vanishes, this term does not appear.

Following the lowest-energy occupied states, the system is ferromagnetic in the vicinity of $k = 0$. At the K point we have degenerate bands with the same spin orientation as the Co

layer, nevertheless, driving a current by means of an external electric field in the graphene plane, one can tune the k_x vector so that two oppositely oriented bands are the lowest occupied bands, making the magnetization ground state zero. So we have magnetic state switching controlled by the charge current on the graphene layer.

Various scenarios of interest can be explored by using, as proposed in Ref. [8], a Cu surface so as to sandwich the graphene layer between Co and Cu. The Cu surface will serve to control the Fermi level and access differently polarized magnetization states as a function of gate voltage and charge current.

IV. CONCLUSIONS

We have derived, within the perturbative tight-binding approximation, the spectral signatures of two Co-graphene registries, the ATOP (one Co atom atop of each A carbon atom) configuration and the HCP (Co at the centers of the hexagonal cells of graphene). Each registry produces a very different spectrum: (i) The ATOP configuration generates a gap in pristine graphene with spin-dependent electron heavy and light effective masses for both the conduction and valence bands that are tunable controlling orbital overlaps. As found by DFT, the graphene layer becomes almost perfectly antiferromagnetic with down-spin orientations at sublattice A and up-spin favored orientation at sublattice B. (ii) The HCP configuration preserves the linear dispersion of graphene, with a small modification of the fermi velocities. The resulting linear dispersions shift in energy according to the spin orientation favoured on the sublattices. For this configuration, ferromagnetic order is preferred and it is parallel to the Co polarization. We have suggested ways to manipulate the magnetic state of the surface by applying a gate voltage (in the work function regime) and by driving a current through the system. There is peculiar coupling between spin and electron momentum induced by the magnetic state of the Co. It amounts to a spin-orbit coupling induced by the driving current. This feature is worth exploring in the future for both its transport and topological implications in graphene nanoribbons.

Using Co and Ni interchangeably in this work is a good approximation as can be judged from detailed DFT calculations [20]. Nevertheless, there are some quantitative differences in the amount of charge transfer and the magnetic moment on the graphene mainly induced by slight changes in the bonding lengths both in the graphene and the interface layer involved. For the ATOP configuration the charge transfers per carbon atom are almost identical between Co and Ni, but the induced magnetization can be two times higher for Ni for small number of layers of the metal. Also the gap induced in the ATOP configuration can be manipulated slightly by changing the number of layers without changing the qualitative picture. It remains to be seen what the corresponding effects are from the HCP configuration.

ACKNOWLEDGMENTS

We thank R. Kiehl for proposing that we address this problem. We acknowledge the hospitality of the Chemistry department of ASU for hosting one of us (E.M.) during a Fulbright Scholarship. B.B. and E.M. acknowledge support from the project PICS-CNRS 2013-2015.

APPENDIX A: DIRECTION COSINE SUMS

The summation $\sum_{m,l=1}^{3}[\hat{n}_{lx}\hat{n}_{lmx}+\hat{n}_{ly}^2\hat{n}_{lmy}]$ is performed as follows: Performing first the sum over l, i.e., over the Co/Ni atoms $l=1,2,3$ as can be seen in Fig. 4, $n_{1x}=0$, because there is no overlap between A and Co in $\hat{x}$ for $l=1$. The other terms are $n_{1y}=-1$, $n_{2y}=n_{3y}=1/2$, and $n_{2x}=-\sqrt{3}/2$, $n_{3x}=\sqrt{3}/2$. Therefore

$$\sum_{l=1}^{3}\sum_{m=1}^{3}(\hat{n}_{lx}\hat{n}_{lmx}+\hat{n}_{ly}\hat{n}_{lmy}) = \sum_{m=1}^{3}\left[-n_{1my}+\frac{n_{2my}+n_{3my}}{2}+\frac{\sqrt{3}}{2}(n_{3mx}-n_{2mx})\right]. \tag{A1}$$

Now, performing the remaining sum, for $m=1$ only the cobalts $l=2$ and $l=3$ intervene, so $n_{11y}=0$, $n_{21y}=n_{31y}=1/2$, and $n_{21x}=\sqrt{3}/2$, $n_{31x}=-\sqrt{3}/2$. Doing the sum for $m=1$ we have

$$m=1:\left[-0+\frac{1/2+1/2}{2}+\frac{\sqrt{3}}{2}\left(-\frac{\sqrt{3}}{2}-\frac{\sqrt{3}}{2}\right)\right]=-1.$$

For $m=2$ only the Co/Ni $l=2$ and $l=1$ intervene, so $n_{12y}=1/2$, $n_{22y}=-1$,$n_{32y}=0$, $n_{22x}=0$, and $n_{32x}=0$. Doing the sum for $m=2$ one obtains

$$m=2:\left[-\frac{1}{2}+\frac{-1+0}{2}+\frac{\sqrt{3}}{2}(0-0)\right]=-1.$$

Finally, for $m=3$ the intervening Co/Ni are $l=1$ and $l=3$, so $n_{13y}=1/2$, $n_{23y}=0$, $n_{33y}=-1$, $n_{23x}=0$, and $n_{33x}=0$. The sum for $m=3$ is then

$$m=3:\left[-\frac{1}{2}+\frac{0-1}{2}+\frac{\sqrt{3}}{2}(0-0)\right]=-1.$$

So in spite of the complicated combination of direction cosines, all the matrix overlaps are equivalent.

APPENDIX B: PARAMETER VALUES OF THE ATOP HAMILTONIAN

From Eq. (22), with $\varepsilon=\varepsilon_p-\varepsilon_d$, one obtains

$$\mu=-\frac{\varepsilon}{2}\left(\frac{V_{pdz}^2}{\varepsilon^2-\delta_1^2}+3\frac{\widetilde{V}_{pd\pi}^2}{\varepsilon^2-\delta_2^2}\right), \tag{B1}$$

$$h_{0z}=\frac{\varepsilon}{2}\left(\frac{V_{pdz}^2}{\varepsilon^2-\delta_1^2}-3\frac{\widetilde{V}_{pd\pi}^2}{\varepsilon^2-\delta_2^2}\right), \tag{B2}$$

$$h_{z0}=\frac{\delta_1 V_{pdz}^2}{\varepsilon^2-\delta_1^2}+3\frac{\delta_2\widetilde{V}_{pd\pi}^2}{\varepsilon^2-\delta_2^2}, \tag{B3}$$

$$h_{zz}=\frac{\delta_1 V_{pdz}^2}{\varepsilon^2-\delta_1^2}-3\frac{\delta_2\widetilde{V}_{pd\pi}^2}{\varepsilon^2-\delta_2^2}. \tag{B4}$$

[1] K. S. Novoselov, V. I. Falko, L. Colombo, P. R. Gellert, M. G. Schwab, and K. Kim, Nature (London) **490**, 192 (2012).
[2] L. Song *et al.*, Nano Lett. **10**, 3209 (2010).
[3] H. Kazi, Y. Cao, I. Tanabe, M. S. Driver, P. A. Dowben, and J. A. Kelber, Mater. Res. Express **1**, 035601 (2014).
[4] D. Marchenko, A. Varykhalov, M. R. Scholz, G. Bihlmayer, E. I. Rashba, A. Rybkin, A. M. Shikin, and O. Rader, Nature Comm. **3**, 1232 (2012).
[5] Z. Wang, C. Tang, R. Sachs, Y. Barlas, and J. Shi, Phys. Rev. Lett. **114**, 016603 (2015).
[6] S. Ostovar pour *et al.*, Nature Chem. **7**, 591 (2015).
[7] S. J. Gong *et al.*, New J. Phys. **12**, 103040 (2010); Appl. Phys. Lett. **100**, 122410 (2012); C. D. Porter and D. Stroud, Phys. Rev. B **85**, 235452 (2012).
[8] H. Chen, Q. Niu, Z. Zhang, and A. H. MacDonald, Phys. Rev. B **87**, 144410 (2013).
[9] M. A. H. Vozmediano, M. P. Lopéz-Sancho, T. Stauber, and F. Guinea, Phys. Rev. B **72**, 155121 (2005).
[10] L. Brey, Phys. Rev. B **92**, 235444 (2015).
[11] J. Balakrishnan, G. Kok Wai Koon, M. Jaiswal, A. H. Castro Neto, and B. Ozyilmaz, Nature Phys. **9**, 284 (2013).
[12] J. C. Slater and G. F. Koster, Phys. Rev. **94**, 1498 (1954).
[13] S. Konschuh, M. Gmitra, and J. Fabian, Phys. Rev. B **82**, 245412 (2010).
[14] E. McCann and M. Koshino, Rep. Prog. Phys. **76**, 056503 (2013).
[15] H. M. Pastawski and E. Medina, Rev. Mex. Fís. **47** (Suppl. 1), 1 (2001); S. Varela, V. Mujica, and E. Medina, Phys. Rev. B **93**, 155436 (2016).
[16] G. Giovannetti, P. A. Khomyakov, G. Brocks, V. M. Karpan, J. van den Brink, and P. J. Kelly, Phys. Rev. Lett. **101**, 026803 (2008).
[17] P. A. Khomyakov, G. Giovannetti, P. C. Rusu, G. Brocks, J. van den Brink, and P. J. Kelly, Phys. Rev. B **79**, 195425 (2009).
[18] E. Clementi and C. Roetti, At. Data Nucl. Data Tables **14**, 177 (1974).
[19] N. Bolívar, E. Medina, and B. Berche, Phys. Rev. B **89**, 125413 (2014).
[20] T. Abtew, B.-C. Shih, S. Banerjee, and P. Zhang, Nanoscale **5**, 1902 (2013).